

# Euler Solutions to Nonlinear Acoustics of Non-Lifting Hovering Rotor Blades

J. D. Baeder

U.S. Army Aviation Research and Technology Activity - AVSCOM  
Aeroflightdynamics Directorate  
NASA Ames Research Center, Moffett Field, California USA

## Abstract

For the first time a computational fluid dynamics (CFD) method is used to calculate directly the high-speed impulsive (HSI) noise of a non-lifting hovering rotor blade out to a distance of over three rotor radii. In order to accurately propagate the acoustic wave in a stable and efficient manner, an implicit upwind-biased Euler method is solved on a grid with points clustered along the line of propagation. A detailed validation of the code is performed for a rectangular rotor blade at tip Mach numbers ranging from 0.88 to 0.92. The agreement with experiment is excellent at both the sonic cylinder and at 2.18 rotor radii. The agreement at 3.09 rotor radii is still very good, showing improvements over the results from the best previous method. Grid sensitivity studies indicate that with special attention to the location of the boundaries a grid with approximately 60,000 points is adequate. This results in a computational time of approximately 40 minutes on a Cray-XMP. The practicality of the method to calculate HSI noise is demonstrated by expanding the scope of the investigation to examine the rectangular blade as well as a highly swept and tapered blade over a tip Mach number range of 0.80 to 0.95. Comparisons with experimental data are excellent and the advantages of planform modifications are clearly evident. New insight is gained into the mechanisms of nonlinear propagation and the minimum distance at which a valid comparison of different rotors can be made: approximately two rotor radii from the center of rotation.

## Introduction

Radiated noise can severely restrict rotorcraft usage in both civilian and military operations. When it occurs, impulsive noise is unquestionably the loudest and the most annoying source of noise. It is annoying because the ear is particularly sensitive to pressure changes that occur over a very short period of time. Impulsive noise can be broken down into two areas: high-speed impulsive noise (HSI), and blade-vortex interaction noise (BVI). BVI noise is very difficult to model due to the importance of unsteady, three-dimensional and wake effects.

HSI noise is usually seen in forward flight but it also appears in hover for high tip Mach numbers. Schmitz and Yu [1] demonstrated that in both cases, a similar curve arises for peak pressure as a function of Mach number when Mach number is taken as the advancing tip Mach number or the hovering tip Mach number, as appropriate. In addition, the influence of lift on HSI noise is secondary. Therefore, this study only examines HSI noise of a non-lifting hovering rotor blade.

At low tip speeds the flow in the vicinity of the rotor blade is purely subsonic. The point at which the

rotational velocity is equal to the undisturbed speed of sound, the linear sonic cylinder, is located far from the blade. As the tip Mach number of the rotor increases the compressibility effects increase and the aerodynamics becomes nonlinear: supersonic pockets form on the rotor blade. In addition, the linear sonic cylinder is now located relatively close to the tip of the rotor blade as displayed in the first part of figure 1. If the tip Mach number is large enough, then the supersonic pocket on the blade may extend out to the supersonic region past the linear sonic cylinder. This delocalization phenomenon was established by Yu et al [2]. The amplitude of the noise increases drastically. In addition, the noise becomes much more impulsive in nature as displayed in the second part of figure 1. Hence, the term high-speed impulsive noise. Unfortunately, the difficulty of properly including these nonlinear effects limited the success of previous attempts to model HSI noise.

## Discussion of Acoustic Methods for HSI Noise

Three different methods have been proposed to model the acoustic propagation of HSI noise: the acoustic analogy approach, the Kirchoff formulation, and computational fluid dynamics.

### Acoustic Analogy Approach

The acoustic analogy approach of Lighthill [3] as developed by Ffowcs Williams and Hawkins (FW-H) [4] is the most commonly used method to model HSI noise. The FW-H equation considers helicopter noise to be broken down into three components: (1) the thickness noise which is generated by the displacement of the fluid as the blade rotates, (2) the loading noise which is generated by the distributed aerodynamic forces on the rotor blade surface and (3) the nonlinear noise which is generated by large gradients in the Lighthill stress tensor. The acoustic analogy approach models the thickness and loading noise by integrating monopole and dipole sources over the surface of the blade, while it models the nonlinear noise by integrating quadrupole sources over the whole volume of the fluid domain.

The main difficulty with the FW-H formulation is that it requires the distribution of sources as an input and it relies on experimental data or numerical calculations from CFD to provide such input. This input must be accurate since second order derivatives are required to calculate the quadrupole terms. Also, the quadrupole calculations are made more tractable through approximations. Usually some of the Lighthill stress tensor terms and all of the acoustic near-field terms are neglected and the domain of the quadrupole integration is made finite. Unfortunately, these approximations require a knowledge of which terms can safely be neglected and exactly how large to make the

domain of the integration. In fact, the limiting of the domain of integration has lead several researchers to question the ability to handle the nonlinear term when the flow becomes delocalized [5-7].

Despite these limitations, many things have been learned about HSI noise using the acoustic analogy approach. Schmitz and Yu [8], using an acoustic planform method in the time domain to solve the FW-H equation and a transonic-small disturbance code to provide the source input for the quadrupole term, demonstrated the importance of the quadrupole term in determining the peak amplitude and shape of HSI noise. Unfortunately, the amplitude of the negative peak pressure is in poor agreement with experiment: tending to underpredict slightly before delocalization and drastically overpredict after delocalization. Prieur [7], using a frequency domain method to solve the FW-H equation, had similar results but was still able to demonstrate the relative effect of the rotor blade planform on HSI noise.

#### Kirchoff Formulation

An alternative method to study HSI noise is to consider a Kirchoff formulation. A linear Kirchoff method requires the control surface to be large enough to contain all of the nonlinear aerodynamic behavior of the problem. Therefore, Isom, et al [9] developed a nonlinear Kirchoff formulation based on the small disturbance potential equation. As in the acoustic analogy approach, there are two linear terms which are surface integrals and a nonlinear term which is a volume integral. However, by using a stationary phase approach with a high frequency assumption, the nonlinear term can be converted to a surface integral at the linear sonic cylinder. This is because in hover the linear sonic cylinder is then a caustic surface where all of the important data originates. Thus, by locating the surface for the two linear terms at the same location, only data on the sonic cylinder is required. The nonlinear Kirchoff formulation propagates this data along linear characteristics to the far-field.

The main difficulty with Isom's formulation is the possible restrictions due to the high frequency assumption. This should result in the underprediction of any low frequency contribution due to the nonlinear term. The neglecting of the nonlinear term when the flow is not delocalized, due to the absence of a shock crossing the sonic cylinder, should also cause an underprediction since the nonlinear contribution to the acoustics is known to be non-negligible. The method also assumes that the curvature of the shock in the plane normal to rotation is negligible, which is not true for very strong shocks.

In spite of the above limitations, important discoveries have been made using this method. Isom's formulation demonstrates that when the flow becomes delocalized the amplitude of the acoustic wave in the far-field should fall off like  $1/\beta$ , where  $\beta$  is the distance along a line tangent to the sonic cylinder as shown in figure 2 [9]. Purcell [10], using a full potential code, was able to get fairly good agreement with experiment at the sonic cylinder. However, the agreement deteriorated some at greater distances from the rotor blade where Isom's equation was

used. Nevertheless, the amplitudes of the negative peak pressures were still within 15 to 20 percent of the experimental values for a rectangular blade with a tip Mach number of 0.90 and 0.92. At tip Mach numbers of 0.88 and lower the agreement was not as good because of the neglecting of the nonlinear term, since the flow is no longer delocalized, as well as the coarsening of the grid near the sonic cylinder. Meanwhile, at tip Mach numbers higher than 0.92 the full potential code had difficulty converging. However, the amplitude of the negative peak pressure would probably be overpredicted since the assumptions that the shock is isentropic and that the curvature of the shock in a plane normal to the plane of rotation is negligible are both no longer valid.

#### Computational Fluid Dynamics

Most CFD methods can be constructed to satisfy the acoustic equations of propagation as well as to calculate the transonic flow field in the vicinity of the rotor blade. Therefore, the use of a purely CFD method has also been proposed to investigate HSI noise. Previously such a method was thought to be impractical, with an accurate solution requiring too large of computer resources. This study demonstrates that it is feasible to extend the domain of a CFD method to the far-field to calculate simultaneously the aerodynamics and the acoustics.

#### Numerical Solution Procedure

The numerical solution procedure of CFD requires the determination of the proper set of governing equations, numerical algorithm, and computational grid.

#### Governing Equations

The choice of governing equations affects the computational time and the level of physics modelled. The aerodynamic flow about rotor blades has been solved over a wide range of governing equations, from lifting-line to Navier-Stokes. The linear methods are clearly not suitable for examining HSI noise since the need to capture the transonic flow field in the vicinity of the rotor blade requires a nonlinear method. However, in order to model HSI noise a nonlinear method must do more than just capture a transonic flow field. The governing equations must accurately model the shock strength, location and curvature as well as the nonlinear propagation of acoustic waves.

The transonic small disturbance (TSD) formulation provides the simplest and computationally most efficient approach to study nonlinear problems. It is derived by eliminating most of the nonlinear terms from the full-potential equation, based on assumptions of the order of the various terms in the vicinity of the rotor blade. However, this elimination of some of the terms based on aerodynamic considerations results in a modified characteristic equation. Because of this, the TSD formulation is not as well suited for studying the nonlinear propagation of acoustic waves. In addition, the shock jump conditions modelled by the TSD formulation limits the method to relatively weak shocks. The

strength of strong shocks is overpredicted and the shocks are located further downstream. Thus, the TSD formulation is unsuitable for studying HSI noise at a distance from the rotor.

The Navier-Stokes equation set is the most complete physical model. The Navier-Stokes and the Euler equations are often solved using the same numerical algorithm, by including or neglecting the viscous terms. However, the resolution of the viscous boundary layer requires a fine grid and results in a very stiff set of equations. These two factors combine to result in larger computer requirements for solving the Navier-Stokes equations. Fortunately, since the noise induced by viscous drag and/or viscous-inviscid interaction is minimal it is not necessary to solve the Navier-Stokes equations to study HSI noise.

The full potential equation correctly models the nonlinear propagation of an acoustic wave exactly. Furthermore, the shock jump conditions are better modelled than for the TSD formulation. However, the shocks are still assumed to be isentropic. Thus, the curvature of shocks is neglected. This results in a slight overprediction of the strength of very strong shocks as well as a location further downstream. The Euler equations model shocks correctly by eliminating the isentropic assumption. They also properly model the nonlinear propagation of acoustic waves as well as the convection of entropy and vorticity. Taking into account all of the above considerations, at a minimum the full potential equation should be used to study HSI noise. However, since very strong shocks are possible, the best choice is to use the Euler equations.

#### Numerical Algorithm

Although the Euler equations properly model the nonlinear propagation of acoustic waves, a numerical algorithm must be implemented that maintains this favorable characteristic when the equations are discretized. At the same time the algorithm must maintain stability in the hyperbolic outer region and keep the computational time reasonable. Fortunately, each one of these considerations does not have to be considered separately. Rather, they are inter-related. Numerical algorithms that take into account more of the fluid physics tend to be more stable and ultimately require less computational time.

Central-difference schemes are well suited for studying flows that are basically elliptic in space, because the stencil assumes that information travels equally in all directions. However, they require artificial dissipation models to stabilize the flow in regions where the flow becomes spatially hyperbolic. Unless the dissipation model is very sophisticated, taking into account what the true domains of dependence and influence should be, too much dissipation is added in some regions and the solution accuracy is degraded. On the other hand, upwind-biased schemes are formed on the basis of the theory of characteristics and attempt to model accurately the propagation of waves as well as the convection of mass, entropy and vorticity. No explicit artificial dissipation models are required to stabilize these schemes. In

addition, no special boundary conditions are required at the far-field since the upwind-biased schemes assure that these boundaries are non-reflecting.

The increased stability of implicit schemes over explicit schemes is desirable to speed up the convergence to a steady-state solution. However, this must be balanced against the increased computational effort per iteration. In order to solve the nonlinear equations implicitly, the equations are linearized. The linearization of the left-hand-side (LHS) is usually limited to the first-order terms and results in a single large-bandwidth matrix. Further approximations are made because of the difficulty of inverting this matrix directly. Usually approximate factorization (AF) in two or three of the spatial directions is performed. However, the inversion of the resulting block-tridiagonal matrices is still time consuming and the factorization errors may limit the stability of the scheme. Therefore, Jameson and Yoon [11] developed an alternate method, LU-SGS, to solve the LHS. The Jacobian terms that result from linearization are simplified such that an LDU factorization can be performed in which only scalar inversions are needed. This drastically reduces the computational effort, to the point where the calculation of the LHS is only a fraction of the total calculation. An additional benefit is an increase in stability due to the reduction in the factorization error.

Chen et al used a finite-volume algorithm based on Roe upwind-biasing with high-order MUSCL-type limiting (third-order accurate in space) on the right-hand-side and the LU-SGS implicit operator on the left-hand-side to calculate the aerodynamics of rotor blades [12]. The code was originally developed to solve the problem in the inertial frame. However, he also demonstrated the ability of the code to calculate the flow in the reference frame of the rotor through the addition of source terms in the momentum equations. The comparison with experiment was excellent. The shocks were well defined with the pressure jump occurring across a maximum of three grid cells.

The algorithm in Chen's code translates the favorable features of the Euler equations (accurate modelling of inviscid shocks and propagating waves) into a discretized form in a computationally efficient manner. Thus, his code is used to undertake the investigation of HSI noise. Since this investigation is limited to rotors in hover, the source terms are included to look at the problem in the steady reference frame of the rotor. This allows for spatial variation of the time-step to accelerate convergence and also eliminates the need to perform Newton iterations.

#### Computational Grid

Once an appropriate set of governing equations and numerical algorithm are chosen it is still necessary to determine the proper computational grid upon which to discretize the problem. A grid topology must be chosen that can accurately model the blade geometry and allow for easy validation with experiment. Furthermore, because a fine distribution of grid points everywhere in the flow domain is computationally prohibitive the grid points

must be clustered in the regions of large gradients and in the regions of most interest.

The basic grid topology chosen is the same as that in the work of Chen et al [12-13]. A cylindrical grid is formed by solving Poisson equations. A planar two-dimensional C-grid is generated at each desired cross-section along the span of the rotor blade and the fictitious extension of the blade. Then, each of the planar grids is deformed to lie at a constant radial distance from the center of the rotor blade's rotation. These grids are stacked together to form a cylindrical C-H grid. This process distorts the blade planform since it results in curved spanwise stations on the blade. The distortion is very small if the planform is rectangular. However, the distortion increases if the blade has sweep and can no longer be neglected since transonic flow is very sensitive to small changes in sweep.

The planform of the two rotor blades to be examined is illustrated in figure 3. Since the DART blade contains significant sweep, Chen's grids were modified. The grid in the vicinity of the rotor blade surface is allowed to remain planar and smoothly blends away from the blade surface into the grid with constant radial sections. This results in the correct planform shape. The constant radial stations away from the blade simplify validation with experiment. The spatial angular variation in pressure along the moving grid corresponds to the temporal variation in pressure measured by a stationary acoustic microphone.

Computational grids for calculating the aerodynamics of rotor blades tend to be highly clustered in the vicinity of the rotor blade surface with a coarse distribution of points away from the blade. Although acceptable for aerodynamic calculations, this is not acceptable for acoustic calculations. A fine distribution of points is also needed away from the blade to capture and propagate the acoustics accurately. However, a fine distribution of grid points in all three directions everywhere in the flow field is not practical. It is also not necessary since the acoustic disturbance is limited to a small region in the vicinity of the linear characteristic curve. The definition of this linear characteristic curve is very simple for a rotor in hover. A fine clustering of points away from the rotor only in the vicinity of this characteristic curve drastically reduces the number of grid points required. It is obtained by rotating the grid sections outboard of the rotor tip such that the clustering of grid points in the fictitious extension of the rotor blade is moved into the region of the linear characteristic curve. The schematic of such a grid in the plane of the rotor blade is illustrated in figure 4. Note that although the cylindrical nature of the grid reduces the skewness of the grid towards the outer boundary, it is still rather large and a potential source of instability or errors. The calculation time is reduced further by calculating only the bottom half of the flow field for non-lifting rotors with symmetric airfoil sections.

#### Validation and Comparison

The high-speed impulsive noise from a non-lifting hovering rotor blade is calculated using the above

numerical solution procedure to determine the validity of such a method for calculating directly the far-field noise. The rotor blade examined is that used in both the experiments of Boxwell et al [14] and Purcell [10]. The blade is a 1/7th scale model of a UH-1H main rotor with straight untwisted blades of constant chord and a NACA 0012 airfoil section. This rotor is 41.14 inches in radius with a 3 inch chord for an aspect ratio of approximately 13.7. The planform of this rectangular rotor blade is shown in figure 3.

The calculations are performed on a C-H grid covering the lower half of the flow field. It consists of 64 points in the wrap-around direction with 46 points on the blade, 59 points in the spanwise direction with 15 points on the blade and 31 points in the normal direction. The inner radial station is located 3.5 chords away from the center of rotation, while the outer radial station is located 43 chords away. The lower grid boundary is located 16 chords below the plane of the rotor. Such a mesh requires slightly more than one hour of Cray2 CPU time to reach convergence.

Due to the importance of delocalization the method is validated against experimental conditions for which the flow is just barely delocalized, not quite delocalized and highly delocalized. Only the experimental results of Purcell are shown because of the similarity to the results of Boxwell et al. Comparisons are also made with previous computations.

#### Rectangular Blade, tip Mach number = 0.90

Experiments establish that at a tip Mach number of 0.90 the rectangular blade is just barely delocalized. Thus, a sharp jump in the pressure is propagated all the way out to the far-field. This is a good test case because a CFD code has never been used before to try to maintain a shock wave out to such large distances. In addition, almost all of the previous methods have calculated the HSI noise of this case to determine their validity to handle such a critical condition as delocalization.

A comparison between experiment and the Euler calculations using a 64x59x31 grid is shown in figure 5 for the time histories at various locations. The agreement with experiment is excellent at both the sonic cylinder and at 2.18 rotor radii. The amplitude of the negative peak pressure is well predicted, within 5% of the experimental values. The sharp pressure jump across the propagating shock wave is clearly evident as well as the initial compression. The width of the wave is also well predicted. Although the agreement at 3.09 rotor radii deteriorates somewhat, it is still very good. Two possible reasons exist for the slight deterioration in agreement at 3.09 rotor radii: the skewness of the grid is starting to affect the accuracy; and/or slight inaccuracies in the calculations are gradually accumulating as one moves so far away from the rotor. However, to keep the amount of the disagreement in perspective one must realize that the difference in the amplitude of the negative peak pressure is still only about 10%, about equal to the amount of error said to be present in such experiments [1].

The results from Purcell [10], using a full potential code and Isom's equation, are also plotted in figure 5. The amplitude of the negative peak pressure and the width of the wave are well predicted by the full potential code at the sonic cylinder. However, the initial compression is somewhat underpredicted and the part of the wave following the sharp compression appears to oscillate incorrectly. Isom's equation is used to propagate the solution to 3.09 rotor radii. At that location the amplitude of the negative peak pressure is underpredicted by almost 20%. The width of the pressure pulse is too narrow and the discrepancies before and after the main acoustic wave remain. Figure 6 compares the predicted amplitude of the negative peak pressure for all of the previous methods to the current method as well as to the experiment. The calculations of Purcell are seen to be much better quantitatively than any of the previous calculations using the acoustic analogy approach (Schmitz and Yu [8], Aggarwal [15] and Prieur [7]). However, the current Euler calculations are now for the first time within the bounds of experimental error.

#### Rectangular Blade, tip Mach number = 0.88

Experiments show that at a tip Mach number of 0.88 the rectangular blade is not yet delocalized. Although the contribution of nonlinearities is non-negligible, the high-frequency content is minimal and as a result the far-field pressure time history is almost symmetrical. Thus, no sharp jump in the pressure is propagated all the way out to the far-field. This is clearly visible in the first part of figure 7 which plots the experimental and computational time histories at 3.09 rotor radii. The shape of the wave is well predicted by the Euler code. In addition, the amplitude of the negative peak pressure is well predicted, within 12% of the experimental value. This difference is half of that due to the predictions of Purcell, possibly because Purcell's calculations neglect the nonlinear term when the flow is not delocalized. Codes using the acoustic analogy approach tend to predict the amplitude of the negative peak pressure fairly well, due to the localized nature of the nonlinearities.

#### Rectangular Blade, tip Mach number = 0.92

When the tip Mach number of the rectangular rotor blade reaches 0.92 the flow becomes highly delocalized. The acoustic analogy methods tend to drastically overpredict the amplitude of the negative peak pressure, by approximately a factor of two. High-frequency content of the acoustic wave is very large with significant nonlinearities. The second part of figure 7 plots the time histories at 3.09 rotor radii for the experiment, the Euler calculations on a 64x59x31 grid and Purcell's calculations. In this case the amplitude of the negative peak pressure is well predicted by both methods (about a 8% difference for both), well within the range of experimental error. The Euler method accurately predicts the shape and width of the negative pressure pulse as well as the initial compression. The over-expansion after the shock wave is not as well predicted. As was the case for a tip Mach number of 0.90, the full potential and Isom's equation method of Purcell predicts a narrower pulse width

and underpredicts the initial compression as well as oscillates after the strong compression wave.

### Grid Sensitivity Studies

In order to assess the dependence of the solution on grid size and the location of the lower grid boundary, two sensitivity studies were performed on the rectangular blade for the case of a tip Mach number of 0.90.

#### Grid Resolution

As mentioned earlier all of the above calculations were performed on a C-H grid consisting of 64 points in the wrap-around direction with 46 points on the blade, 59 points in the spanwise direction with 15 points on the blade and 31 points in the normal direction, requiring approximately one hour of Cray2 CPU time and seven million words of memory. The solutions using the above grid were found to be very accurate when compared to experiment. Thus, the effect of grid resolution is studied by decreasing the number of grid points in the hope that fewer grid points might still give adequate results.

The original grid was used to generate three smaller grids. The smallest considered consists of every other grid point in every direction of the original grid (1/8 as many grid points) or a 31x30x16 grid with 23x8 points on the rotor blade surface. The next smallest grid keeps all of the grid points in the normal direction, but discards every other grid point in the wrap-around and spanwise directions. This results in a 31x30x31 grid with 23x8 points on the rotor blade surface. The largest of the three smaller grids discards only every other grid point in the spanwise direction of the original grid, resulting in a 64x30x31 grid with 46x8 points on the rotor blade surface.

As stated earlier, when the flow is delocalized the amplitude of the acoustic wave in the far-field is inversely proportional to the tangential distance to the sonic cylinder,  $\beta$ . Therefore, Figure 8 plots the amplitude of the scaled negative peak pressure (scaled by multiplying by  $\beta$ ) versus  $\beta$ . As expected, the two experimental values display the relative insensitivity of this scaled pressure with distance. The original fine grid solution indicates an initial increase in the scaled pressure with distance but then is relatively constant between values of  $\beta$  between 1.5 and 2.5. After a value of  $\beta$  greater than 2.5 the scaled pressure starts to decrease, probably indicating that the growing skewness of the grid is introducing numerical error. Yet the error at 3.09 rotor radii is still within experimental bounds. The largest of the three smaller grids (half as many points in the spanwise direction) results in a nearly identical curve. However, the additional dropping of every other point in the wrap-around direction and then in the normal direction causes the accuracy of the solution to deteriorate drastically. The smallest grid predicts a negative peak pressure at 2.18 rotor radii that is only two-thirds of the amplitude of the experimental value. In addition, the time histories displayed in figure 9 indicate that the initial compression and the over-expansion after the shock wave are not well predicted. Note, that the decreased resolution in the

spanwise direction has almost no effect on the time history.

Thus, it appears that the solution is least sensitive to the number of grid points in the spanwise direction. This is not surprising, since the outer portion of the grid is rotated such that the clustering of points follows the acoustic wave. The largest gradients in the flow field tend to lie in the wrap-around direction and the direction normal to the plane of rotation. This grid sensitivity study indicates that a 64x30x31 grid with 46x8 points on the grid surface is adequate to predict high-speed impulsive noise of a non-lifting rotor blade in hover. This results in a grid of approximately 60,000 grid points and a computational time of approximately 40 minutes on a Cray-XMP using less than four million words of main memory.

#### Grid Boundary Location

As mentioned previously, all of the above calculations are performed on a C-H grid with the lower grid boundary located 16 chords from the plane of the rotor. However, original calculations to study the HSI noise were performed on the same 64x59x31 grid but with the lower boundary located only 8 chords below the plane of the rotor.

The change in the location of this boundary has a negligible effect on the time histories at the sonic cylinder and at 2.18 rotor radii. However, if this boundary is located only 8 chords from the plane of the rotor the time history at 3.09 rotor radii is distorted. This is visible in figure 10, for a tip Mach number of 0.90. The solution now contains an unphysical bump in the time history in the region following the shock wave. The same trend is visible in solutions for tip Mach numbers of 0.88 and 0.92. The unphysical bump in the solution is most likely due to a small reflection off the lower grid boundary. Thus, the effect of the reflection is only visible at larger radial distances by which time the reflected wave reaches the plane of the rotor. By moving this boundary farther away the amplitude of the reflection is decreased and the location of the point that such a weaker reflected wave reaches the plane of the rotor is moved radially outward. Although the location of the lower grid boundary has almost no effect on the amplitude of the negative peak pressure it is still best to place this boundary at least 16 chords from the plane of the rotor.

#### Results for Two Planform Shapes

It is one thing to demonstrate the ability of a code to predict accurate results on a few selected test cases for a very simple geometry. However, the true usefulness of a method is its applicability to more complex geometries and a wide range of operating conditions. Therefore, to demonstrate the usefulness and practicality of the Euler method for calculating HSI noise the scope of the investigation is expanded. The rectangular rotor blade as well as the swept-tip DART (Drag and Acoustic Rotor Test) rotor blade is investigated for tip Mach numbers

ranging from 0.80 to 0.95. Both planforms are illustrated in figure 3.

The exact geometry of the DART blade is given in the paper by Bridgeman, et al [16]. The DART rotor uses an extensive parabolic sweep which gives an approximately constant leading edge normal Mach number outboard of 0.75 rotor radii. The rotor employs NACA 00XX profiles which taper from 12% thickness at 0.75 rotor radii to 9.5% thickness at the tip. The rectangular blade solutions are performed on the 64x59x31 grid mentioned previously, while the DART blade solutions are performed on a 64x30x31 grid with 46x8 points on the blade surface. Increasing the number of grid points in the spanwise direction for the DART blade solutions has a negligible effect.

#### Comparison with Experiment

Purcell conducted the acoustic test of the DART rotor blade in hover [17]. The DART blade was found to delocalize at a tip Mach number of approximately 0.91, only slightly higher than for the rectangular blade. However, the amplitude of the peak negative pressure was found to be one-third to one-half of that due to the rectangular blade over a tip Mach number range of 0.90 to 0.95. Purcell also performed acoustic calculations using the full potential code and Isom's equation [17]. The amplitude of the negative peak pressure at 2.18 rotor radii was underpredicted by 15 to 30% and there was a large overshoot of the positive peak due to the overexpansion of the shock when the flow became delocalized.

The amplitudes of the negative peak pressures for experiment and the Euler method are plotted in figure 11 versus tip Mach number for the two blade planforms. The experimental rectangular blade data is that measured at 3.09 rotor radii, while the DART blade experimental data is that measured at 2.18 rotor radii and scaled by 1/3 to predict that at 3.09 rotor radii (only data at 2.18 rotor radii is available for the DART blade experiment). The computed data for both blades is that predicted by the Euler code at 3.09 rotor radii. The agreement between the Euler method and experiment is excellent for the rectangular rotor blade, with a difference between the two of less than 12% for all of the various tip Mach numbers considered. The agreement between data from the Euler code and the DART blade experiment is not as good but the difference is still less than 30%. The Euler code was found earlier to seem to become less accurate after 2.18 rotor radii. Thus, a direct comparison between the experimental and computed values at 2.18 rotor radii reveals that the differences at that location are only 5 to 15%.

#### Comparisons With Each Other

It has already been noted that the change in planform of the DART blade relative to the rectangular blade reduces the amplitude of the negative peak pressure as well as delays the onset of delocalization. The calculations down to a tip Mach number of 0.80 reveal that even at such relatively moderate tip speeds the DART blade exhibits reduced acoustic noise. However, a comparison of the

computed time histories at the sonic cylinder and at 2.18 rotor radii, plotted in figure 12 and 13, also reveals that the DART blade does not show any initial compression wave. This is also visible in the experimental time histories [17]. The lack of the initial compression is probably due to the fact that the sweep in the tip region provides more spanwise flow which relieves the compression in the leading edge region. This decreases the pressure drag in the tip region as is visible in the aerodynamic calculations of Bridgeman, et al [16].

The time histories at the sonic cylinder indicate that when the flow is delocalized, the amplitude of the negative peak pressure from the DART blade is just as large as that due to the rectangular blade. However, the width of the pulse is much smaller due to the decreased chord in the tip region. The smaller pulse width results in a stronger gradient in the expansion wave. As the waves propagate outward, nonlinearities cause the steeper expansion wave from the DART blade to flatten more and the width of the pulse to increase faster. Thus, by the time that the acoustic waves reach 2.18 rotor radii the widths of the pulses from the two blades are comparable. Furthermore, the amplitude of the negative peak pressure from the DART blade becomes much smaller when compared to that from the rectangular blade. This indicates that a comparison of only the amplitude of the negative peak pressure close to the blade is not enough if the flow is delocalized, the width of the pulse is also important since that also affects the acoustic intensity.

The scaled negative pressure peak is plotted versus the tangential distance to the sonic cylinder in figure 14 for the two blades at tip Mach numbers ranging from 0.88 to 0.95. Before the onset of delocalization, the plots indicate that this function increases gradually and monotonically with distance to its far-field values. In addition, the values are very close to the far-field values by the time that  $\beta$  approaches values of one. However, once the flow becomes delocalized this function no longer increases monotonically. Rather, initially the function increases rapidly with distance due to the strong contribution from the nonlinear sources near the sonic cylinder. Then, the function decreases as the strong expansion wave flattens and the pulse width becomes wider. Because the DART blade initially has a steeper expansion wave and smaller pulse width, this effect is more pronounced. This effect is also more pronounced as the flow field becomes more delocalized. The far-field values are not approached until  $\beta$  reaches values of almost two, corresponding to at least two rotor radii from the center of rotation.

### Conclusions

This work demonstrates that with special attention to the numerical solution procedures the use of a purely CFD method to calculate high-speed impulsive noise is not only feasible, but practical as well. For the first time, CFD calculates the HSI noise out to a distance of slightly over three rotor radii over a wide range of tip Mach numbers for two different planforms. The comparison to date with experimental data is very encouraging with excellent agreement, better than any other existing method. The detailed information available increases the understanding

of HSI noise by gaining new insight into the mechanisms of nonlinear propagation and how far away from the rotor one must be to make a valid comparison of different rotors: a distance of approximately two rotor radii from the center of rotation if the flow becomes delocalized.

Future work will concentrate on extending the method to forward flight and to cases with lift. The extension to forward flight is relatively straight forward. The only difficulty concerns the proper gridding of such a problem. The unsteady motion of the blade relative to the acoustic wave requires a time-adaptive grid to maintain the clustering of the grid in the vicinity of the acoustic wave. The extension to lifting rotor blades is more difficult since it requires the accurate inclusion of the effects of the wake. It also requires better resolution in the part of the grid away from the plane of rotation. However, once a lifting rotor in forward flight is calculated it will be possible to begin examining the feasibility of using CFD methods to examine blade-vortex interaction noise.

### References

1. Schmitz, F. H. and Yu, Y. H., "Helicopter Impulsive Noise: Theoretical and Experimental Status," NASA TM 84390 and USAAVRADCOTR 83-A-2, November 1983.
2. Yu, Y. H., Caradonna, F. X., and Schmitz, F. H., "The Influence of the Transonic Flow Field on High-Speed Helicopter Impulsive Noise," Paper No. 58, 4th European Rotorcraft Forum, Italy, 1978.
3. Lighthill, M. J., "On Sound Generated Aerodynamically," Philosophical Transactions of the Royal Society, A564, 1952.
4. Ffowcs Williams, J. E. and Hawkins, D. L., "Sound Generated by Turbulence and Surfaces in Arbitrary Motion," Philosophical Transactions of the Royal Society, A264, 1969.
5. Isom, M. P., "Some Non-Linear Problems in Transonic Helicopter Acoustics," Poly M/AE Report 79-19, Polytechnic Institute of New York, May 1979.
6. Morris, C. E. K. Jr., Farassat, F., and Nystrom, P. A., "An Evaluation of Linear Acoustic Theory for a Hovering Helicopter," NASA TM 80059, May 1979.
7. Prieur, J., "Calculation of Transonic Rotor Noise Using a Frequency Domain Formulation," AIAA Journal, Vol. 26, No. 2, February 1988, pp. 156-162.
8. Schmitz, F. H. and Yu, Y. H., "Transonic Rotor Noise - Theoretical and Experimental Comparisons," Vertica, Vol. 5, 1981, pp. 55-74.
9. Isom, M. P., Purcell, T. W. and Strawn, R. C., "Geometrical Acoustics and Transonic Helicopter Sound," AIAA 87-2748, AIAA 11th Aeroacoustics Conference, Sunnyvale, California, 1987.

10. Purcell, T. W., "CFD and Transonic Helicopter Sound," Paper No. 2, 14th European Rotorcraft Forum, Milan, Italy, 1988.
11. Jameson, A. and Yoon, S., "Lower-Upper Implicit Schemes with Multiple Grids for the Euler Equations," AIAA Journal, Vol. 25, No. 7, July 1987, pp. 929-935.
12. Chen, C. L., McCroskey, W. J., and Obayashi, S., "Numerical Solutions of Forward-Flight Rotor Flow Using an Upwind Method," AIAA 89-1846, AIAA 20th Fluid Dynamics, Plasma Dynamics and Lasers Conference, Buffalo, New York, 1989.
13. Chen, C. L., and McCroskey, W. J., "Numerical Simulation of Helicopter Multi-Bladed Rotor Flow," AIAA 88-0046, AIAA 26th Aerospace Sciences Meeting, Reno, Nevada, 1988.
14. Boxwell, D. A., Yu, Y. H., and Schmitz, F. H., "Hovering Impulsive Noise: Some Measured and Calculated Results," NASA CP-2052, 1978, and Vertica, Vol. 3, No. 1, 1979.
15. Aggarwal, H. R., "The Calculation of Transonic Rotor Noise," AIAA Journal, Vol. 22, No. 7, July 1984, pp. 996-998.
16. Bridgeman, J. O., Strawn, R. C., Caradonna, F. X. and Chen, C. S., "Advanced Rotor Computations with a Corrected Potential Method," 45th Annual Forum of the American Helicopter Society, Boston, Mass., 1989.
17. Purcell, T. W., "A Prediction of High-Speed Rotor Noise," AIAA 89-1130, AIAA 12th Aeroacoustics Conference, San Antonio, Texas, 1989.

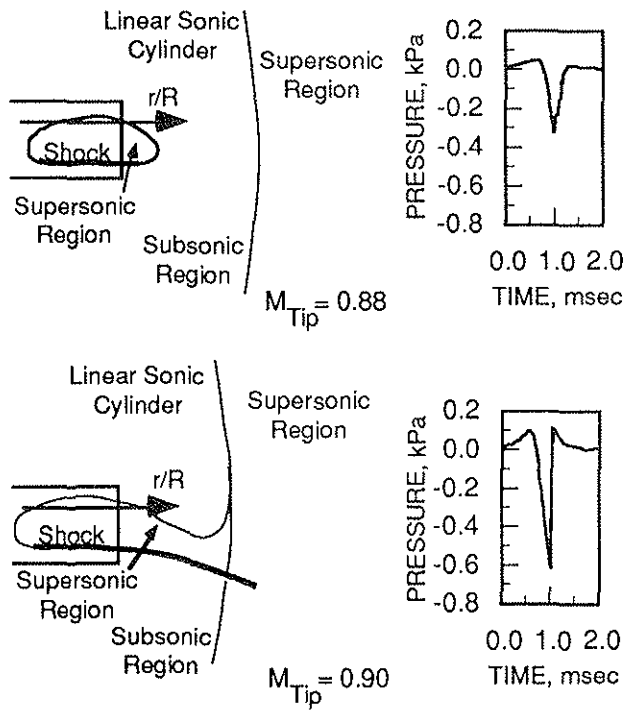


Fig 1. Delocalization.

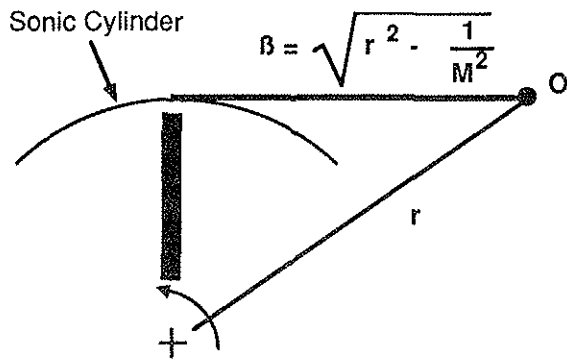
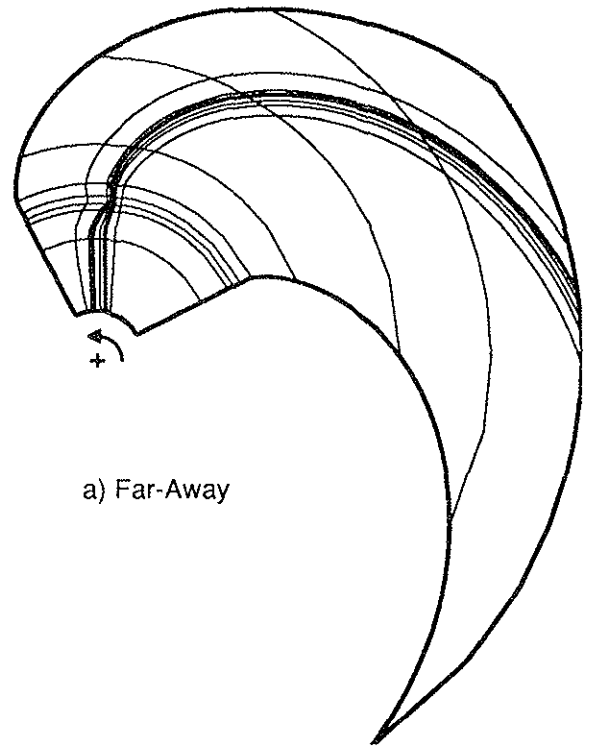


Fig 2. Definition of the parameter  $\beta$  and its relationship to the radial distance and the location of the sonic cylinder.

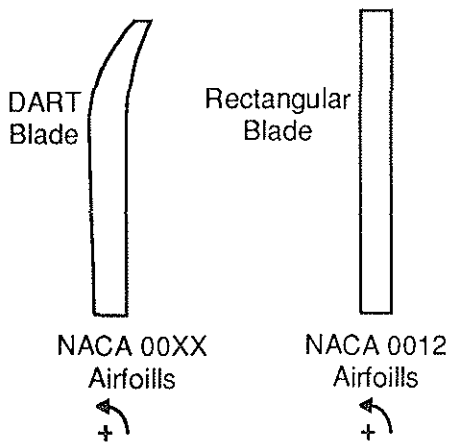


Fig 3. Rotor blades examined.

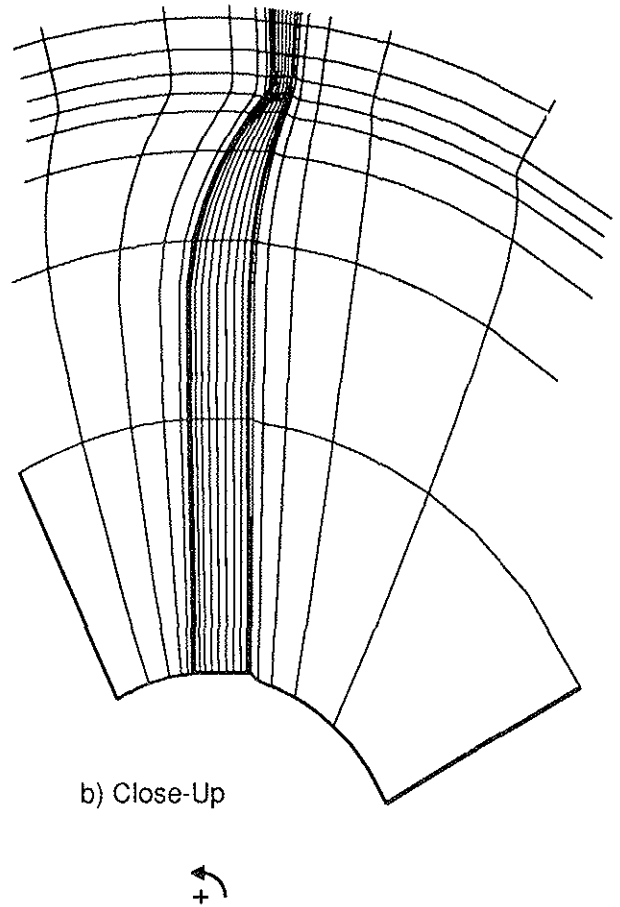


Fig 4. Schematic of grid in the plane of the rotor blade.

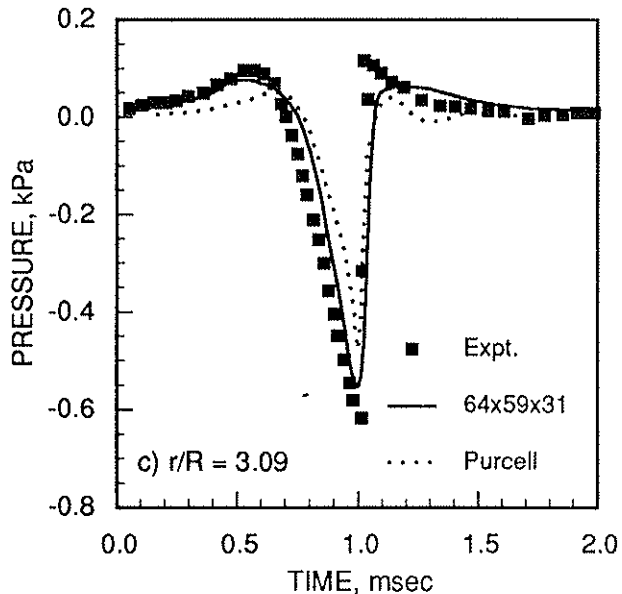
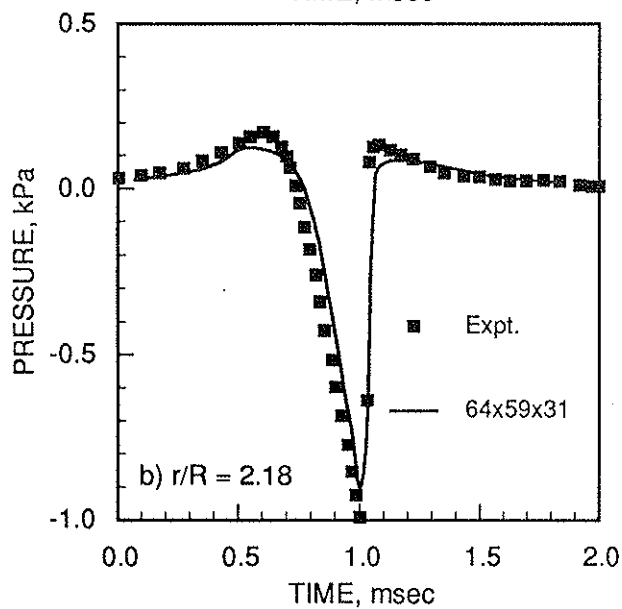
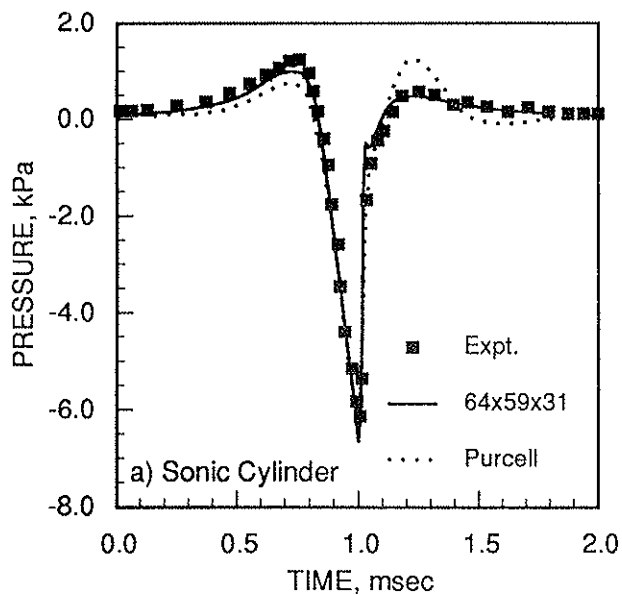


Fig 5. Time histories at various locations for a rectangular blade with tip Mach number of 0.90.

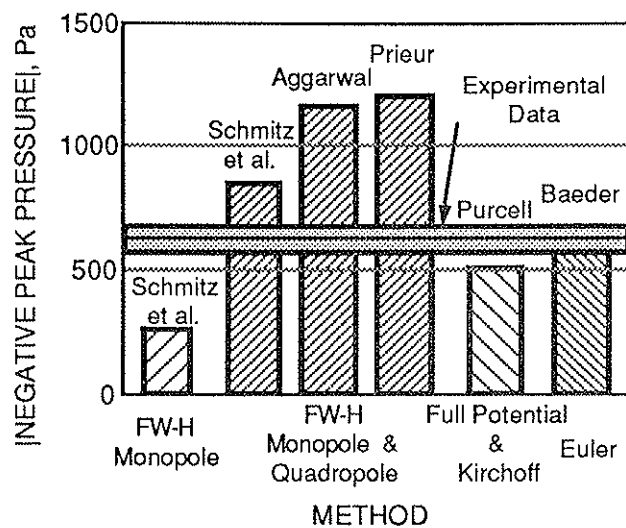


Fig 6. Comparison with experiment and earlier methods of the [negative peak pressure] for rectangular blade with tip Mach number of 0.90,  $r/R = 3.09$ .

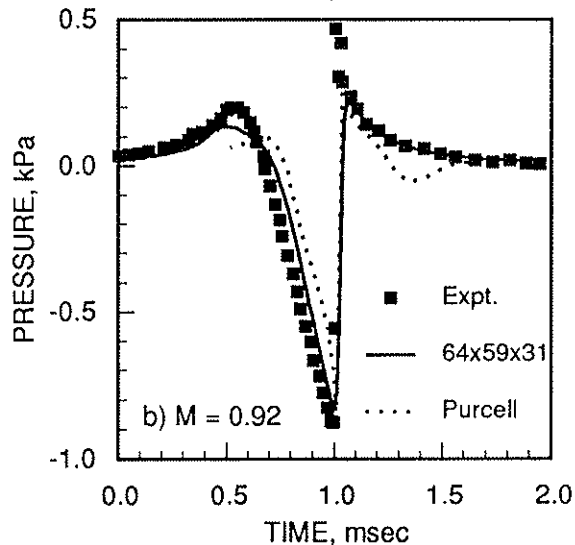
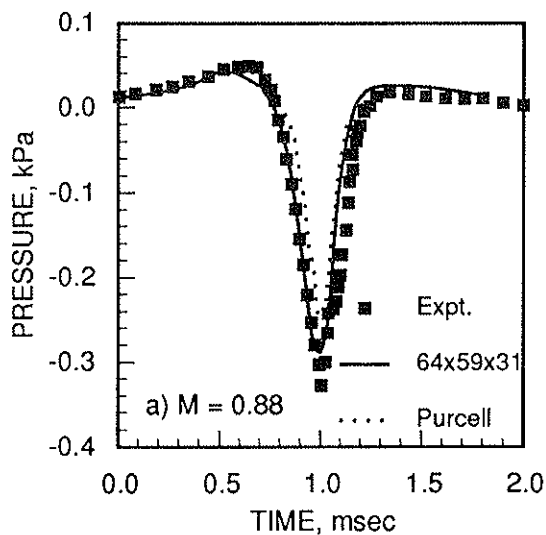


Fig 7. Time histories at  $r/R = 3.09$  for a rectangular blade with two different tip Mach numbers.

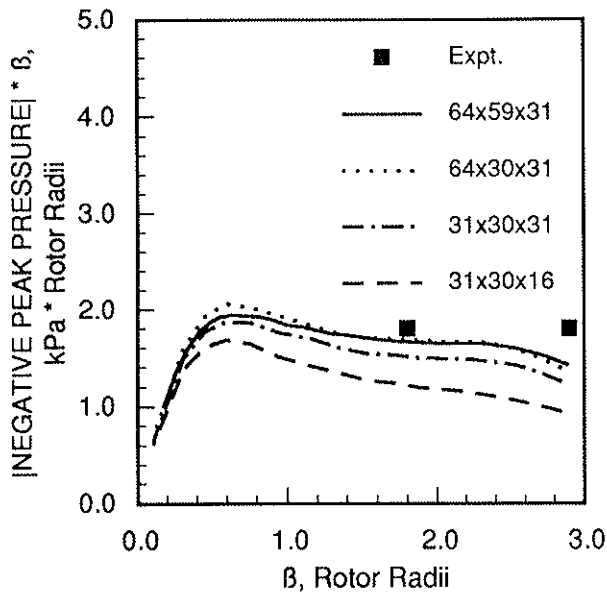


Fig 8. Effect of grid size on the scaled |negative peak pressure| versus distance for a rectangular blade with a tip Mach number of 0.90.

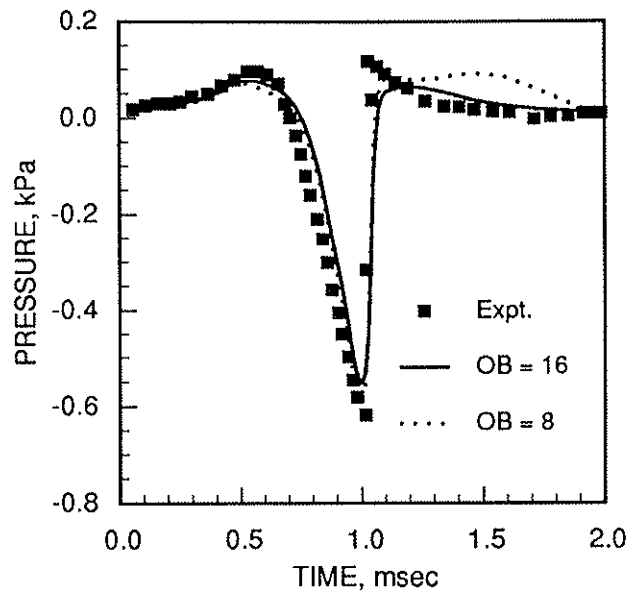


Fig 10. Effect of lower outer grid boundary location on the time history at  $r/R = 3.09$  for a rectangular blade with a tip Mach number of 0.90.

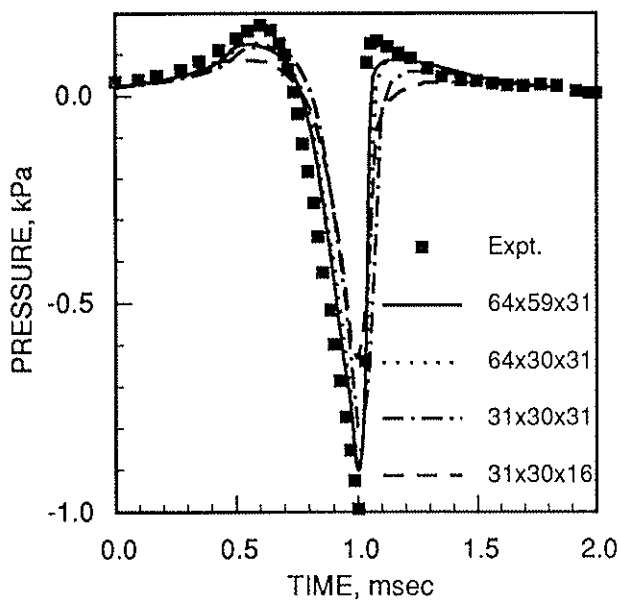


Fig 9. Effect of grid size on the time history at  $r/R = 2.18$  for a rectangular blade with a tip Mach number of 0.90.

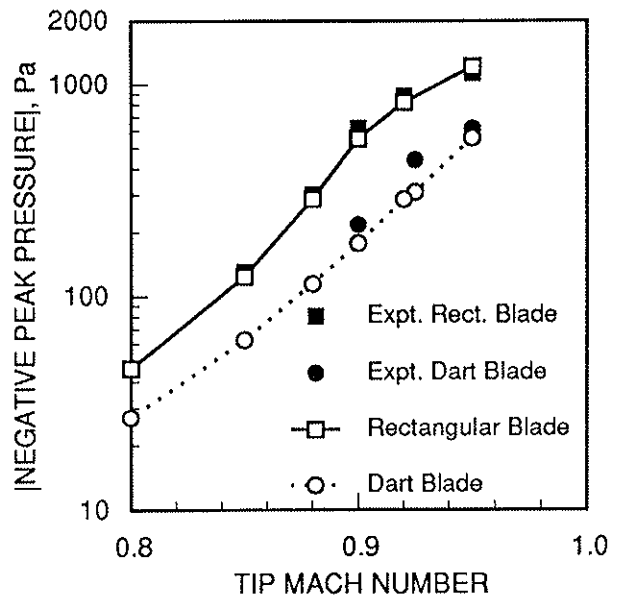


Fig 11. Comparison with experiment of the |negative peak pressure| versus tip Mach number for the rectangular and DART blades at  $r/R = 3.09$ .

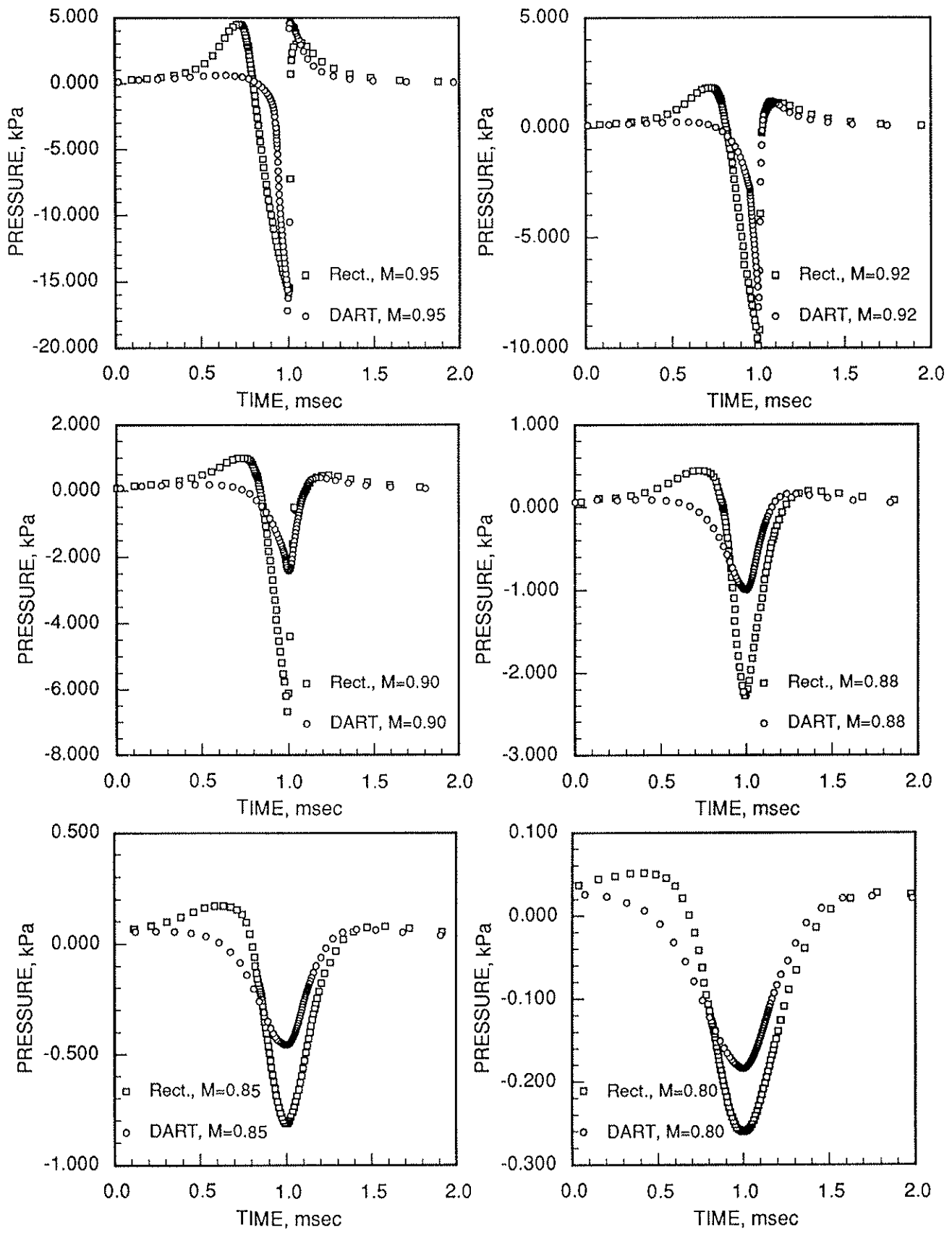


Fig 12. Comparison between the rectangular and DART blades of the computed time histories at the sonic cylinder at various tip Mach numbers.

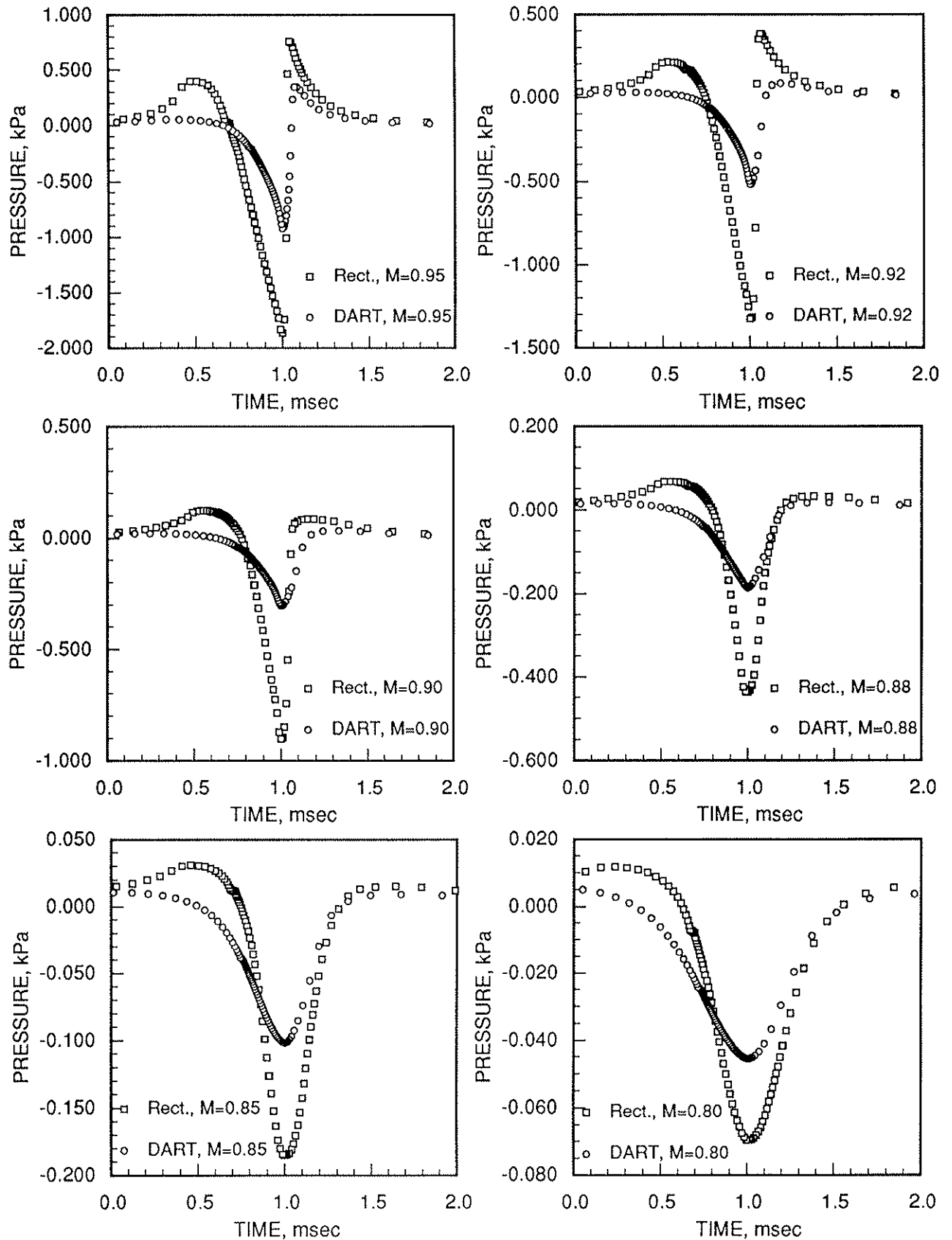


Fig 13. Comparison between the rectangular and DART blades of the computed time histories at  $r/R = 2.18$  at various tip Mach numbers.

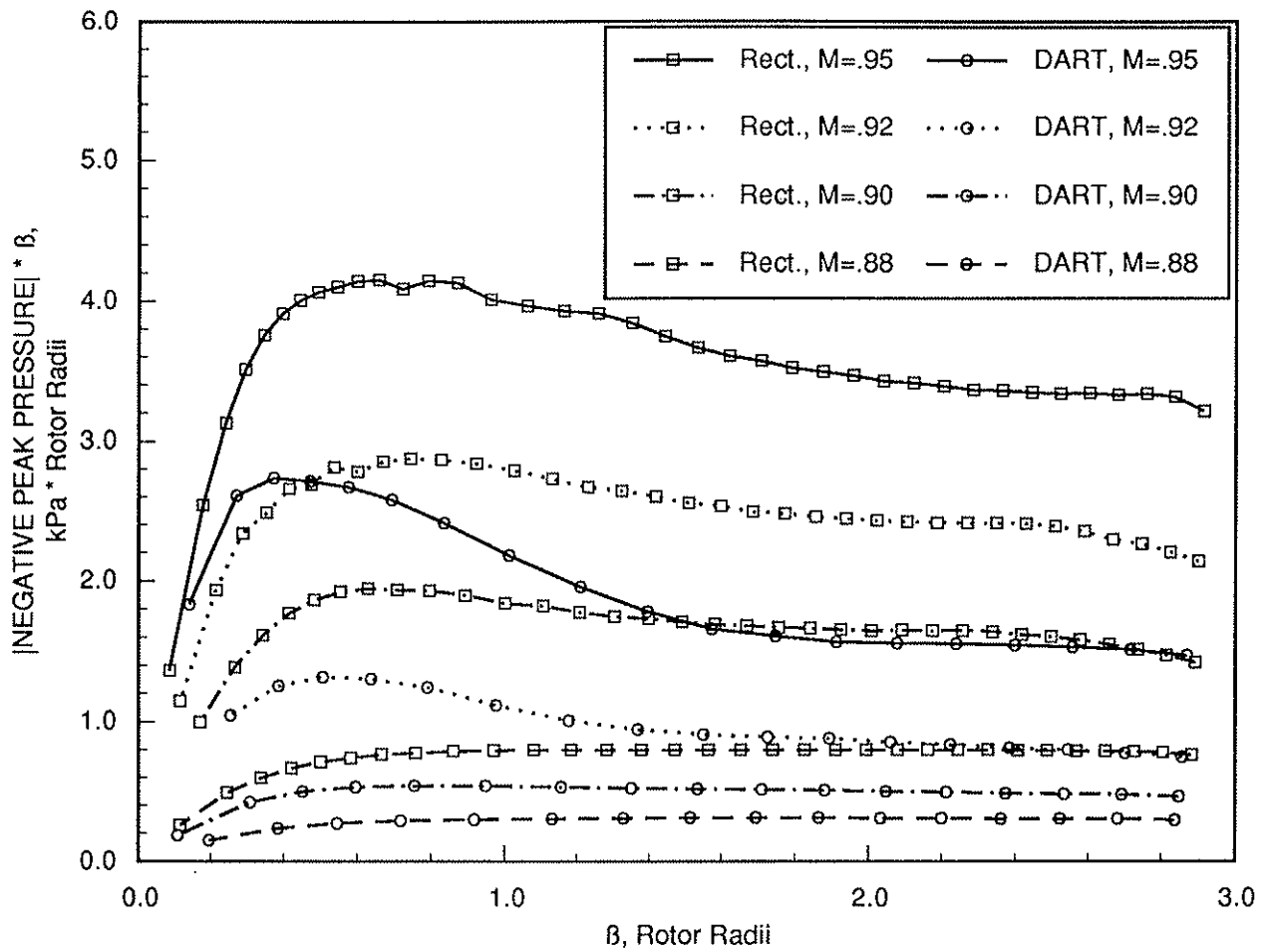


Fig 14. Comparison between the rectangular and DART blades of the computed scaled |negative peak pressure| versus distance at various tip Mach numbers.